Thin Solid Films 519 (2011) 2627–2632

Contents lists available at ScienceDirect

Thin Solid Films

journal homepage: www.elsevier.com/locate/tsf

Selective sensitivity of ellipsometry to magnetic nanostructures

K. Postava [a,*], D. Hrabovský [a], J. Hamrlová [a], J. Pištora [a], A. Wawro [b], L.T. Baczewski [b], I. Sveklo [c], A. Maziewski [c]

[a] Department of Physics, Technical University of Ostrava, 17, listopadu 15, 70833 Ostrava-Poruba, Czech Republic
[b] Institute of Physics, Polish Academy of Sciences, Al. Lotnikow 32/46, 02-668 Warsaw, Poland
[c] Laboratory of Magnetism, Faculty of Physics, University of Bialystok, 41 Lipowa Street, 15-424 Bialystok, Poland

ARTICLE INFO

Available online 10 December 2010

Keywords:
Generalized ellipsometry
Magneto-optical ellipsometry
Material sensitivity
Magnetic nanostructures

ABSTRACT

Magneto-optic (MO) ellipsometry of ferromagnetic materials is extremely sensitive to ultra-thin films, multilayers, and nanostructures. It gives a possibility to measure all components of the magnetization vector in the frame of the magneto-optic vector magnetometry and enables us to separate magnetic contributions from different depths and materials in nanostructures, which is reviewed in this article. The method is based on ellipsometric separation using the selective MO Kerr effect. The figure of merit used to quantify the ellipsometric selectivity to magnetic nanostructures is defined on the basis of linear matrix algebra. We show that the method can be also used to separate MO contributions from areas of the same ferromagnetic materials deposited on different buffer layers. The method is demonstrated using both: (i) modeling of the MO ellipsometry response and (ii) MO measurement of ultra-thin Co islands epitaxially grown on self-organized gold islands on Mo/Al_2O_3 buffer layer prepared using the molecular beam epitaxy at elevated temperatures. The system is studied using longitudinal (in-plane) and polar (perpendicular) MO Kerr effects.

1. Introduction

Complexity of recent magnetic nanostructures requires improvement of characterization techniques and development of new measurement procedures. Among nondestructive and noninvasive techniques, the ellipsometric methods propose high sensitivity to films with thicknesses down to an atomic layer. Magneto-optical (MO) effects, *i.e.* change of optical properties originating from magnetized state of materials, enable applications of ellipsometric methods to magnetic measurement. The magneto-opticalellipsometry profits from all advantages of standard ellipsometry and moreover it is less affected by surface roughness and nonmagnetic films in a structure.

Basic application of MO ellipsometry is the *hysteresis loop measurement* based on detection of the MO signal proportional to magnetization as a function of external magnetic field. The method is used to monitor the magnetization reversal, magnetic anisotropy, hysteresis properties etc. [1]. Its combination with microscopic observation, often called *Kerr microscopy* [2], is used to observe magnetic domains during magnetization reversal. Despite observed domain size being limited by the resolution of optical microscopy, the Kerr microscopy has significantly contributed to the understanding of domain nucleation and domain wall motion. Important information related to electronic structure of a material is obtained from spectral dependence of MO effect. *Magneto-optic spectroscopic ellipsometry* usually based on modulation technique can be combined with standard ellipsometry to obtain spectral dependence of the complete permittivity tensor. Specific techniques based on MO ellipsometry are *ultrafast magneto-optics*, *Brillouin light scattering* [3], or *second harmonic MO generation*.

All the abovementioned applications of MO ellipsometry techniques profit from high near-surface sensitivity, nondestructive character, and possibility to measure all components of the magnetization vector in the frame of the magneto-optic vector magnetometry [4,5]. Moreover, the magneto-optic Kerr effects enable us to separate magnetic contributions from different depths [6–10] and from different materials [11,12] in multilayer systems and self-organized nanostructures [13].

In this paper, the MO ellipsometry is applied to characterize cobalt ultra-thin film deposited on self-assembled gold islands on Mo buffer layer. Selective sensitivity of both the longitudinal and polar MO effect to ferromagnetic Co grown on Au islands and Co grown directly on Mo buffer in the nanostructure is demonstrated experimentally and explained using model. In Section 2 we review some aspects of MO ellipsometry and MO vector magnetometry crucial for measured data understanding and processing for selectively sensitive MO ellipsometry. Section 3 deals with depth and material sensitivity of MO ellipsometry, procedure of separation of MO effect from different phases, and definition of the figure of merit for the separation. Section 4 presents the main original results of MO selective sensitivity

* Corresponding author.
E-mail address: kamil.postava@vsb.cz (K. Postava).

0040-6090/$ – see front matter © 2011 Elsevier B.V. All rights reserved.
doi:10.1016/j.tsf.2010.11.073

affected by buffer layer. Separation of magnetic contribution is explained using model and processing of experimental MO data of Co film grown on nanostructured Au/Mo buffer.

2. Magneto-optical ellipsometry

In this section we define the magneto-optical angles, discuss basic MO configurations and possibility of magnetization component separation in the frame of the MO vector magnetometry [4]. Careful separation of magnetization components and different MO effects is the first step, which precedes to separation of contributions from different materials.

2.1. Basic definitions

Usual description of MO response of a sample is based on the Jones reflection matrix

$$\mathbf{R} = \begin{bmatrix} r_{ss} & r_{ps}(M_P, M_L) \\ r_{sp}(M_P, M_L) & r_{pp}(M_T) \end{bmatrix}, \quad (1)$$

where $r_{ij}, i,j = s,p$ denote the amplitude reflection coefficients. The ratios of the off-diagonal and diagonal reflection coefficients are used for the definition of two MO ellipsometric angles

$$\frac{r_{sp}}{r_{ss}} = tan\,\psi_{sp} exp\left(i\Delta_{sp}\right) = \frac{tan\,\theta_s + i\,tan\,\epsilon_s}{1 - i\,tan\,\theta_s\,tan\,\epsilon_s} \approx \theta_s + i\epsilon_s, \quad (2)$$
$$\frac{r_{ps}}{r_{pp}} = tan\,\psi_{ps} exp\left(i\Delta_{ps}\right) = \frac{tan\,\theta_p + i\,tan\,\epsilon_p}{1 - i\,tan\,\theta_p\,tan\,\epsilon_p} \approx \theta_p + i\epsilon_p.$$

The first forms define the generalized ellipsometric angles $\psi_{sp,ps}$ (related to the amplitudes) and $\Delta_{sp,ps}$ (represent the phases) defined in Refs. [14–16]. Similar definitions were also used in Refs. [17–19]. Note that the ratio $r_{pp}/r_{ss} = tan\psi exp(i\Delta)$ defines the standard ellipsometric angles [20]. The second definition of the magneto-optic angles $\theta_{s,p}$ and $\epsilon_{s,p}$ has clear meaning: for the incident linear polarizations in the s and p direction, the reflected light is elliptically polarized with the slight azimuth rotation $\theta_{s,p}$ and ellipticity $\epsilon_{s,p}$. The mode conversion originates for isotropic sample from the magneto-optic effect. Only experiments measuring both quantities can provide complete ellipsometric information about the MO effect. The MO angles are mostly much smaller than 1 degree and therefore using the approximate formulas in Eq. (2), the MO rotation and ellipticity can be represented as the real and imaginary parts of the complex ellipsometric ratios. Then the quantities $\theta_{s,p}, \epsilon_{s,p}$ and $\psi_{sp,ps}, \Delta_{sp,ps}$ represent the complex ellipsometric ratios in the Cartesian and polar coordinates, respectively. Precise measurement of such small angles usually requires specific ellipsometric configurations different from the standard one or from the Mueller matrix polarimeter, which usually equivalently distribute experimental and calibration errors between components of the Mueller matrix. Frequently used MO ellipsometry configurations use: (i) differential intensity measurement based on Wollaston prism and differential signal between two photodetectors, (ii) polarization modulation technique using the photoelastic modulator (PEM), and (iii) the azimuth modulation and nulling method based on Faraday modulator cells. Another aspect of the MO ellipsometry is the measurement of MO angle differences related to given magnetization state (usually saturated state by external magnetic field).

Small amplitude of MO effect has also important consequences in *additivity* of various MO contributions. MO effect can be usually understood as a small perturbation of optical properties (for instance small anisotropy or gyrotropy) originating from magnetization in materials. Therefore, the total MO effect can be obtained as addition of particular contributions. Here we consider MO contributions from different depths, films, materials, constituents, etc. Additivity of MO effects will be used in Sections 3 and 4 for the separation of different materials in magnetic nanostructure. This linear approximation is usually fulfilled (in all cases discussed in this paper) and it can be confirmed by a model.

2.2. Magneto-optic vector magnetometry

Contributions of different magnetization components (usually mixing of polar and longitudinal MO effects) appear in a similar way as the contributions from different materials. Therefore, an important task of magneto-optical ellipsometry is the careful separation of different magnetization components. We usually distinguish three basic components of the magnetization vector (see Fig. 1): the polar component M_P is perpendicular to the film (surface), the transverse component M_T is perpendicular to the plane of incidence, and the longitudinal one lies in the plane of film and in the plane of incidence. Dependencies of the amplitude reflection coefficients on different magnetization components are schematically shown in Eq. (1). We note that discussion here is restricted to linear MO effects in systems with cubic or higher symmetry, the effects of quadratic MO terms were discussed in Refs. [5,21,22]. The transverse Kerr effect can be observed only using the r_{pp} reflection coefficient [23].

On the other hand, both the longitudinal and polar Kerr effect can be monitored using the conversion reflection coefficients r_{sp}, r_{ps}, or using the MO angles defined by Eq. (2). For their separation, one can use property of in-plane longitudinal and transversal effect, which disappear for normal incidence (for films with higher symmetry). However, changing the angle of incidence can be inconvenient and exactly normal incidence is hard to be used experimentally. Another possibility is based on different symmetries of polar and longitudinal Kerr effects [24]. An interesting method was proposed by Ding et al. [25] based on two measurements for reversed incidence geometries. In this paper, we use modified approach based on rotation of the sample and magnetic field around the sample normal by the angle of 180°. Fig. 2a,b shows two configurations used for polar and longitudinal MO effect separation by addition and subtraction of both measured signals, respectively. Note that both the sample and also the magnetic field have to be rotated. Daboo et al. [26,27] proposed to measure both in-plane magnetization components by rotation of the sample and magnetic field by 90°. The method has significant advantage of direct comparison of both components, because both are measured using the longitudinal MO effect. Therefore, measurements of four sample orientations shown in Fig. 2 result in the separation of three magnetization components denoted by M_P, M_L, and M_T. Table 1 summarizes the effects of the sample and magnetic field rotation on different off-diagonal permittivity tensor elements. The polar MO effect is symmetric by 180° rotation, while longitudinal and transverse effects are antisymmetric. Note that the quadratic (second-order) effect related to product $M_L M_T$

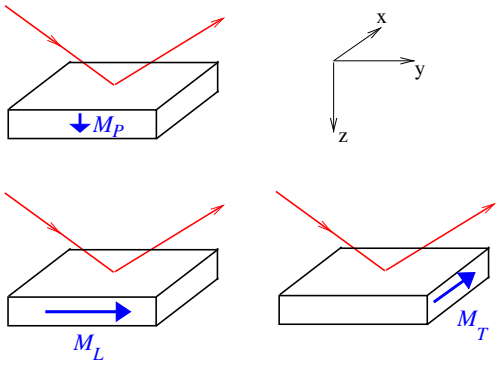

Fig. 1. Basic MO configurations — polar, longitudinal and transverse components of magnetization vector.

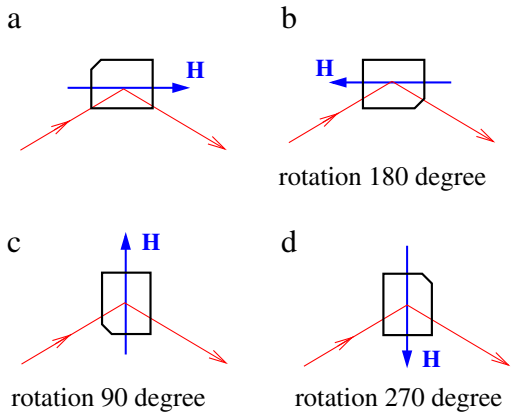

Fig. 2. Separation of the magnetization components using sample rotation. Magnetic field has to rotate together with the sample.

appears in ε_{xy}, has the same symmetry as the polar MO effect (see Table 1), and can be separated from the longitudinal one [28].

3. Selective sensitivity of MO ellipsometry

In this section, the basic principle of MO selective sensitivity is described using an example of depth sensitivity in reflection from a magneto-optic bulk material. We discuss the extension of the method to distinguish MO contributions from constituents in nanostructures (periodic multilayers or self-organized nanostructures).

3.1. Basis of MO selectivity to magnetic nanostructures

Basic idea of MO selective sensitivity is demonstrated on the case of depth sensitivity of the MO effect in a cobalt bulk. The model is based on additivity of MO effects discussed in Section 2.1. Fig. 3 shows a model of magneto-optical ultrathin (1 Å thick) Co film buried in non-magneto-optic Co bulk in the depth t. The similar modeling was originally proposed by Traeger [6] and Hubert [7]. Fig. 3 shows the complex polar Kerr effect obtained for normal incidence. The upper subplot of Fig. 3 shows dependence of the Kerr rotation θ and ellipticity ϵ as a function of the buried MO film depth. While the sensitivity of the rotation θ monotonically decreases due to absorption in Co, the ellipticity ε shows more complex behavior and even changes sign. The different behavior is essential for depth selective sensitivity and comes from phase change by propagation through Cobalt above the film. Even more illustrative is a plot in the complex magneto-optic plane, where the x and y axis correspond to θ and ϵ, respectively (lower subplot of Fig. 3). Each point corresponds to the film in different depth. The points far from the origin represent films close to the surface, while the points close to the origin correspond to deeper films (amplitude of the effect decrease due to absorption and limited penetration depth). However, also the phase of the complex MO effect changes, which is used for depth selectivity. For example two vectors show contributions from different depths. We note that optimal separation is obtained for perpendicular vectors of the same length.

Table 1
The off-diagonal permittivity tensor components as a function of sample rotation φ used for magneto-optic vector magnetometry. Transformation of permittivity tensor was obtained by rotation of the coordinate system around z-axis. Component notation corresponds to the coordinate system shown on Fig. 1.

	Measured by	$\varphi=0°$	$\varphi=90°$	$\varphi=180°$	$\varphi=270°$
ε_{xy}	r_{sp}, r_{ps}	$\varepsilon_{xy}(M_P)$	$\varepsilon_{xy}(M_P)$	$\varepsilon_{xy}(M_P)$	$\varepsilon_{xy}(M_P)$
ε_{xz}	r_{sp}, r_{ps}	$\varepsilon_{xz}(M_L)$	$-\varepsilon_{yz}(M_T)$	$-\varepsilon_{xz}(M_L)$	$\varepsilon_{yz}(M_T)$
ε_{yz}	r_{pp}	$\varepsilon_{yz}(M_T)$	$\varepsilon_{xz}(M_L)$	$\varepsilon_{yz}(M_T)$	$-\varepsilon_{xz}(M_L)$

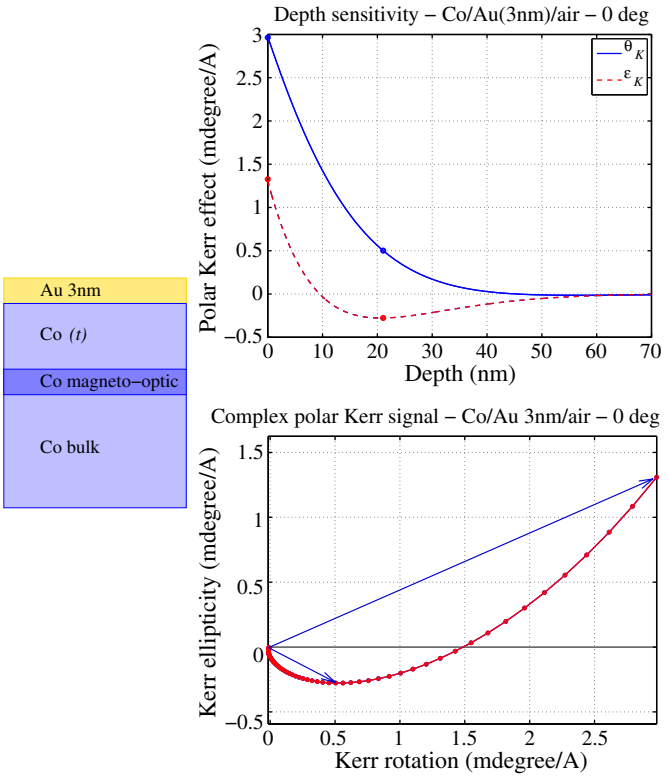

Fig. 3. Depth sensitivity to Co buried layer in nonmagnetic Co bulk for normal-incidence polar Kerr effect. Optical and magneto-optical constants of Co were taken for 670 nm from Refs. [29,30].

Based on the previously discussed dependence of the Kerr rotation and ellipticity one can separate contributions from different depths using several methods. One possibility is to adjust some parameter (the angle of incidence, wavelength [8]) in such a way that the measured MO quantity becomes insensitive to the contribution from one depth and only sensitivity to desired depth remains. However, this method is not very convenient because of complicated alignment of the parameter. A more effective technique was proposed by Ferré et. al [8,9] using adjustable compensating element into the MO ellipsometer. The authors used the Babinet-Soleil compensator, which enables continuous transformation of the Kerr rotation into ellipticity and vice versa. Such adjustment corresponds to rotation of the complex MO plane (lower subplot of Fig. 3) around the origin. Despite general applicability, the method requires several repetition of measurement and difficult adjustment of the compensator parameter. Another approach, used in this paper, is based on a post-measurement data processing by linear combination of all measured MO quantities. Significant advantage of this method, described in details in next subsection, comes from flexible numerical adjustment of weight coefficients after measurement.

Magneto-optical depth sensitivity was used for various systems. Separation of polar MO signal from films in different depth was presented by Ferré et al. [8] and Hamrle et al. [9] in the case of Co films separated by Au spacer. The authors demonstrated separation from hysteresis loops of different Co layers showing different coercivity. The depth sensitivity of longitudinal Kerr effect in Fe/Cr/Fe structure was demonstrated by Nývlt [31]. The depth sensitivity of soft x-ray resonant magneto-optical Kerr effect was reported by Lee et al. [32] and Kim et al. [33]. Moreover, energy adjustment of the x-ray resonant magnetic scattering can give element specific sensitivity [34].

Selective sensitivity of the complex MO effect was obtained also for nanostructures consisting of different magnetic materials [11–13]. Material selective sensitivity of polar magneto-optic Kerr effect was

described and experimentally demonstrated in NiFe/Au/Co/Au multilayers [11]. Despite the fact that the ferromagnetic NiFe and Co layers alternate in the multilayer structure, we were able to separate magnetic response of Co and NiFe films using MO measurements. Such possibility originates from different optical and MO constants of both materials and consequently their different phases in the complex MO plane.

Material selectivity of MO ellipsometry was also observed in self-organized nanostructures. In Ref. [13] we demonstrated material selective sensitivity of a MO polar Kerr effect to magnetic contributions from different inclusions in self-organized magnetic nanostructures. The method is supported by modeling of the magneto-optic response based on the effective medium approximation and by hysteresis loop measurement of the multiferroic $BiFeO_3$–$CoFe_2O_4$ (BFO–CFO) self-assembled nanostructure. On the other hand, the longitudinal MO Kerr effect was applied to distinguish contribution of Fe nanocrystal from amorphous soft magnetic matrix in near-surface region of FeNbB amorphous ribbons [35,36].

3.2. Methods for separation of different contributions

Separation of MO effects from the different depths or materials is obtained in three steps [11,13]: (i) measurement of different MO quantities (for example the MO Kerr rotation θ and ellipticity ϵ) showing different sensitivity to the contributions, (ii) determination of weight coefficients from the model of the structure or from some knowledge of magnetic behavior, and (iii) numerical separation of contributions from different depth or materials in the nanostructure. This section describes this procedure in details.

Based on additivity of MO effects the obtained signals can be expressed as weighted sums of MO contributions from different magnetic phases. Here we describe dependence of the Kerr rotation θ and ellipticity ϵ on two magnetic phases, however generalization to more measured quantities (different incident polarizations, angles of incidence, or inspected light wavelengths) and more magneto-optic phases is straightforward. Based on linearity $\theta = a_1 m_1 + a_2 m_2$ and $\epsilon = b_1 m_1 + b_2 m_2$, where m_1 and m_2 are the normalized magnetizations of two phases. It is convenient to write the relations in the matrix form:

$$\Phi = \begin{bmatrix} \theta \\ \varepsilon \end{bmatrix} = \begin{bmatrix} a_1 & a_2 \\ b_1 & b_2 \end{bmatrix} \begin{bmatrix} m_1 \\ m_2 \end{bmatrix} = \mathbf{AM}, \tag{3}$$

where Φ represents the vector consisting of measured signals by different MO quantities, **M** is the vector of normalized magnetizations of different phases in the structure, and the matrix **A** contains the weight coefficients. The length of the vector **M** has to be less than or equal to the length of the vector Φ. In the following we expect the same length and squareness of the matrix **A**. If we determine the elements of the matrix **A**, which will be discussed later, the magnetization of both phases can be obtained using the matrix inversion:

$$\mathbf{M} = \mathbf{A}^{-1}\Phi. \tag{4}$$

There are two aspects of the inversion (4). Firstly, the procedure to determine elements of matrix **A** is discussed. We have two possibility: (i) calculation of the weight constants $a_{1,2}$ and $b_{1,2}$ from a model, which is straightforward, but it is affected by precision of input optical, magneto-optical, and geometric parameters of the structure. In many cases of practical interest the model is approximate and gives only qualitative agreement with the experiment. Therefore we often use the second possibility (ii) estimation of weight coefficients in the **A** matrix directly from experimental data using our knowledge of magnetic behavior of magnetic phases [11,13]. We, for example know, that for maximal external magnetic field both magnetic phases are saturated and we may expect that for a certain field one phase is already saturated, while the other is not. Separation on this basis was applied in Refs. [11,13].

Secondly, we have to care, whether the matrix inversion $\mathbf{A}^{-1}$ is mathematically possible and how the experimental errors in the measurement of Φ and imperfect determination of the matrix **A** influence errors in obtained **M**. It is clear, that if two vectors in the complex MO plane (see Fig. 3) are collinear (both MO quantity is identically sensitive to two magnetic phases), the lines in the matrix **A** are linearly dependent. The matrix is singular and inversion is not possible. On the other hand, if the vectors in the complex MO plane are perpendicular, the matrix is well conditioned and the matrix inversion can be calculated. We can define the figure of merit describing possibility of magnetic phases separation using the *matrix condition number* $\kappa(\mathbf{A})$.

When we measure the MO effect Φ with the tolerance $\Delta\Phi$, then relative error of magnetic contributions

$$\frac{\|\Delta\mathbf{M}\|}{\|\mathbf{M}\|} \le \kappa(\mathbf{A}) \frac{\|\Delta\Phi\|}{\|\Phi\|} \tag{5}$$

is proportional to the condition number $\kappa(\mathbf{A})$ [37,38]

$$\kappa(\mathbf{A}) = \|\mathbf{A}^{-1}\|\|\mathbf{A}\| = \frac{\sigma_{\max}(\mathbf{A})}{\sigma_{\min}(\mathbf{A})}, \tag{6}$$

where $\|\mathbf{A}\|$ is the norm of the matrix **A**. In our calculations we used the spectral norm [37,38] and the condition number is expressed from the ratio of the maximal $\sigma_{\max}(\mathbf{A})$ and the minimal $\sigma_{\min}(\mathbf{A})$ singular numbers obtained from the singular value decomposition of the matrix **A**. $\kappa(\mathbf{A})$ is closed to 1 for well conditioned matrix and magnetic contributions are well separated. However, for large $\kappa(\mathbf{A})$, the MO ellipsometry is not selectively sensitive to different magnetic phases [36].

4. Experimental demonstrations

This section deals with demonstration of the selective sensitivity in the case of ferromagnetic cobalt film deposited on the self-organized Au islands on the Mo buffer layer. Fig. 4 shows schematically the sample structure. The sample was grown on a monocrystalline sapphire (11$\bar{2}$0) substrate in molecular beam epitaxy (MBE) system. The Au islands are self-assembled on the 20 nm thick Mo(110) epitaxial layer at elevated temperature of 500 °C. Such patterned buffer was covered by the ferromagnetic Co (0001). The measured data presented in this paper were obtained for Co film thickness of approximately 2 nm. The system was capped by 5 nm thick Au film to protect Co from oxidation. Therefore, two ferromagnetic subsystems

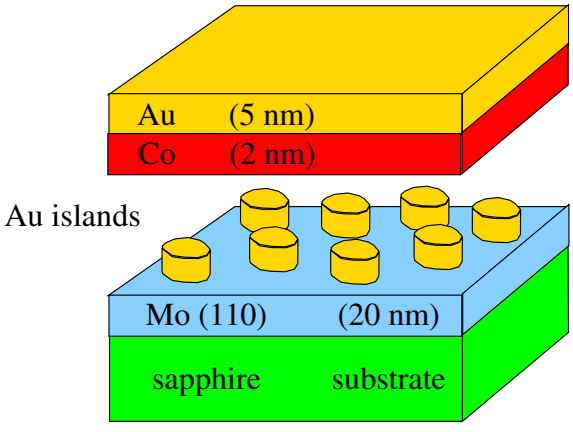

Fig. 4. Schematic plot of the sample structure of Co grown on self-assembled Au islands.

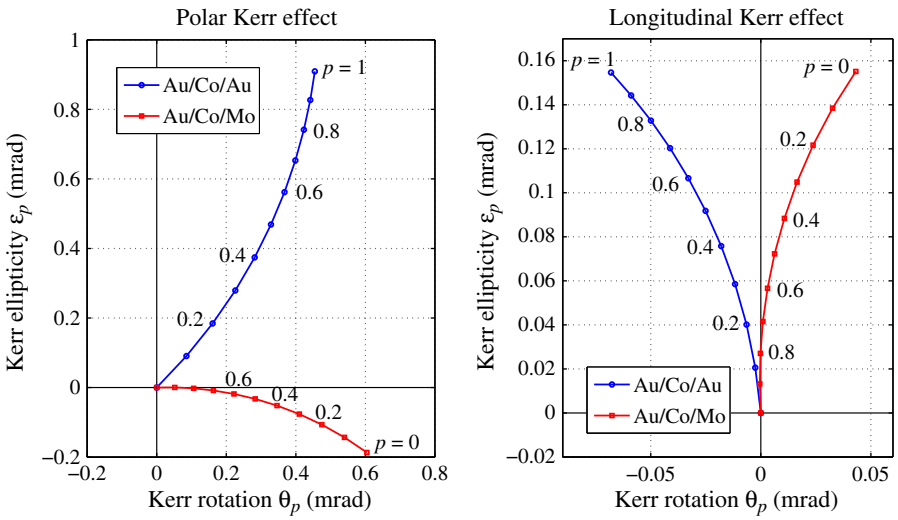

Fig. 5. Contributions to Kerr rotation and ellipticity of Au/Co/Au islands and Au/Co/Mo surrounding are modeled and plotted in the complex MO plane.

coexist in the sample: (i) Au/Co/Au sandwiches — for the part where the Co layer is deposited on the Au islands and (ii) Au/Co/Mo sandwich — as the Co layer is grown between islands on the surrounding Mo surface. Direct growth of Co on Mo buffer results in uniaxial magnetic anisotropy originating from lattice mismatch between Co and Mo [39].

MO selective sensitivity of the sample was modeled using coherent summation of contribution from both subsystems. The total Jones matrix (Eq. (1)) was obtained by weighted summation of particular Jones matrices of $\mathbf{R}_{Au/Co/Au}$ and $\mathbf{R}_{Au/Co/Mo}$:

$$\mathbf{R} = p\mathbf{R}_{Au/Co/Au} + (1-p)\mathbf{R}_{Au/Co/Mo}, \tag{7}$$

where p is the surface fraction of Au islands. MO angles were calculated from the total $\mathbf{R}$ using Eq. (2). Fig. 5 shows the modeled MO contributions of both magnetic fractions in the complex MO plane as a function of the surface fraction p. Left and right subplots represent the polar and longitudinal Kerr effects, respectively. Blue circles and red squares correspond to contributions of Co on gold islands and Mo buffer, respectively. Both the polar and longitudinal MO effects show clear possibility of selective sensitivity to two magnetic subsystems.

The sample was studied using MO Kerr ellipsometer based on differential intensity detection. Semiconductor laser beam of wavelength 670 nm modulated using Polarizer/PEM/Polarizer system at 100 kHz incident at the angle of incidence of 60° on the sample. Polarization of the reflected beam is measured using the achromatic quarter-wave compensator and the Wollaston prism with two detector systems. In-plane direction of external magnetic field is computer controlled together with motorized rotation of the sample. In this paper, we present data obtained for p-polarized incident light.

Fig. 6 shows MO hysteresis loops after separation of all three components of the magnetization vector measured using the Kerr

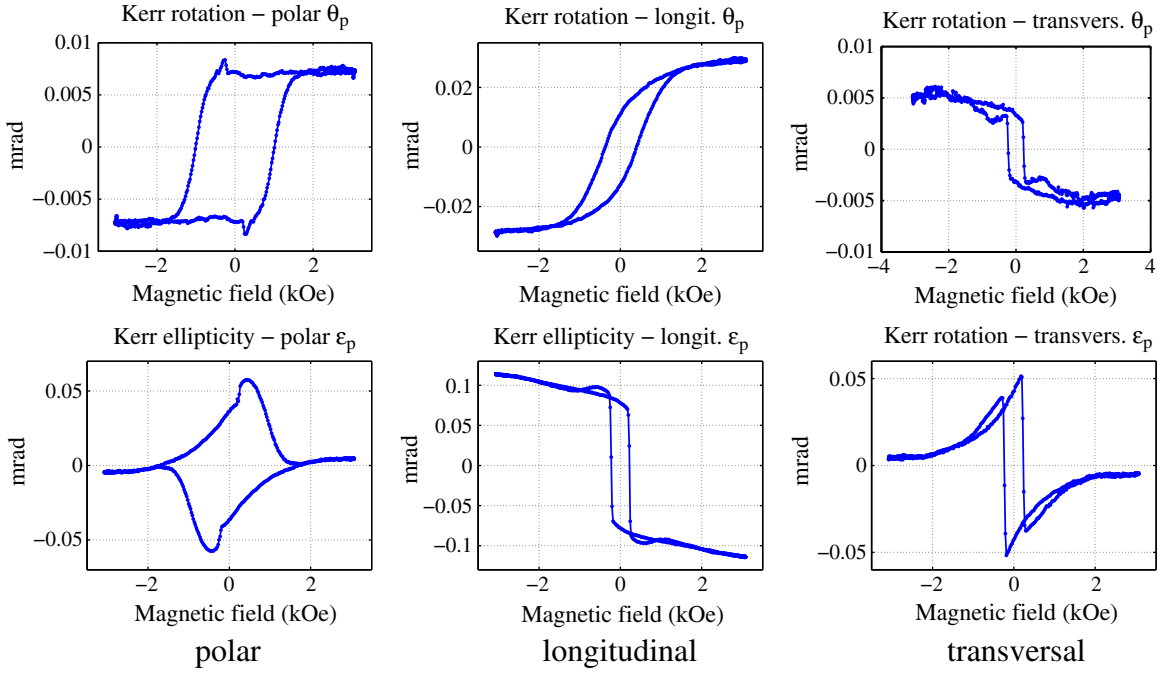

Fig. 6. Separated MO hysteresis loops for p-polarized incident light measured using θ_p (first line) and ε_p (second line). Three columns correspond to polar, longitudinal, and transverse contributions separated using procedure described in Section 2.1.

rotation θ_p and ellipticity ϵ_p (separation procedure is described in Section 2.2, Fig. 2). The loops obtained using the Kerr rotation θ_p (upper line in Fig. 6) are significantly different from the loops of the Kerr ellipticity ϵ_p. Therefore, existence of two contributions from different magnetic systems is clearly evident. We suppose that the upper θ_p-loops come mainly from the Au/Co/Au islands. They contribute also to the lower ϵ_p-loops, but the effects of the surrounding Cobalt deposited on Mo buffer dominate in the lower ϵ_p-loops. In the following we discuss the magnetic behavior: (i) both magnetic phases exhibit the polar magnetization components for in-plane magnetic field. However, the polar components are relatively small and the magnetizations are only slightly inclined out of the plane. (ii) Co grown on Mo buffer shows coherent magnetization rotation and strong in-plane magnetic anisotropy, which is explained by lattice mismatch [39]. (iii) Longitudinal loop for Au/Co/Au islands is wider and smoother indicating the higher coercitive field its distribution for individual islands.

5. Conclusions

Magneto-optical selective sensitivity is described on the basis of rigorous modeling and experimental observation in ultrathin Co films on nanostructure of self-assembled gold islands. Despite the fact that the lateral dimension of nanostructure is smaller than inspected light wavelength, we are able to separate magnetic response of Co deposited on Au island and on surrounding Mo buffer. Such possibility originates from different MO phase resulted from the effect of buffer layer, which significantly affects also magnetic properties. The presented method is general and we believe that it is applicable for various systems of multilayers, periodic structures, and nanocomposites measured by different MO effects.

Acknowledgements

Partial support is from the projects KAN 400100653 (Grant Agency of Academy of Sciences of the Czech Republic), the project N N507 452134 funded by the Ministry of Science and Higher Education in Poland in 2008–2011, MSM6198910016 (Ministry of Education of the Czech Republic), and CZ.1.05/2.1.00/01.0040 (RMTVC), and SP/2010150 is acknowledged.

References

[1] Z.Q. Qiu, S.D. Bader, J. Magn. Magn. Mater. 200 (1999) 664.
[2] A. Hubert, R. Schäfer, Magnetic Domains: The Analysis of Magnetic Microstructures, Springer, Berlin, 1998, p. 369,, Ref. 818.
[3] J. Hamrle, J. Pištora, B. Hillebrands, B. Lenk, M. Munzenberg, J. Phys. D Appl. Phys. 43 (2010) 325004.
[4] Š. Višňovský, R. Lopušník, M. Bauer, J. Bok, J. Rassbender, B. Hillebrands, Opt. Express 9 (2001) 121.
[5] K. Postava, J. Pištora, T. Yamaguchi, Sens. Actuators A 110 (2004) 242.
[6] G. Traeger, L. Wenzel, A. Hubert, Phys. Status Solidi A 131 (1992) 201.
[7] A. Hubert, G. Traeger, J. Magn. Magn. Mater. 124 (1993) 185.
[8] J. Ferré, P. Meyer, M. Nyvlt, S. Visnovsky, D. Renard, J. Magn. Magn. Mater. 165 (1997) 92.
[9] J. Hamrle, J. Ferré, M. Nývlt, Š. Višňovský, Phys. Rev. B 66 (2002) 224423-1.
[10] L.C. Sampaio, J. Hamrle, A. Mougin, J. Ferre, F. Garcia, F. Fettar, B. Dieny, A. Brun, Phys. Rev. B 70 (2004) 104403.
[11] K. Postava, I. Sveklo, M. Tekielak, P. Mazalski, A. Maziewski, A. Stupakiewicz, M. Urbaniak, B. Szymański, F. Stobiecki, IEEE Trans. Magn. 44 (2008) 3261.
[12] P. Vavassori, V. Bonanni, A. Busato, D. Bisero, G.G.A.O. Adeyeye, S. Goolaup, N. Singh, C. Spezzani, M. Sacchi, J. Phys. D Appl. Phys. 41 (2008) 134014.
[13] K. Postava, D. Hrabovský, O. Životský, J. Pištora, N. Dix, R. Muralidharan, J.M. Caicedo, F. Sánchez, J. Fontcuberta, J. Appl. Phys. 105 (2009) 07C124.
[14] M. Schubert, T.E. Tiwald, J.A. Woollam, Appl. Opt. 38 (1999) 177.
[15] M. Schubert, T. Hofmann, C.M. Herzinger, J. Opt. Soc. Am. A 20 (2003) 347.
[16] M. Schubert, Thin Solid Films 313–314 (1998) 323.
[17] G.E. Jellison, Thin Solid Films 450 (2004) 42.
[18] I. Ohlídal, D. Franta, Ellipsometry of thin film systems, in: E. Wolf (Ed.), Progress in Optics, volume 41, North-Holland, Amsterdam, 2000, p. 181.
[19] L. Halagačka, K. Postava, M. Foldyna, J. Pištora, Phys. Status Solidi A 205 (2008) 752.
[20] R.M.A. Azzam, N.M. Bashara, Ellipsometry and Polarized Light, 2nd editionNorth-Holland, Amsterdam, 1987.
[21] Š. Višňovský, J. Phys. B 36 (1986) 1424.
[22] K. Postava, D. Hrabovský, J. Pištora, A.R. Fert, Š. Višňovský, T. Yamaguchi, J. Appl. Phys. 91 (2002) 7293.
[23] K. Postava, A. Maziewski, A. Stupakiewicz, A. Wawro, L.T. Baczewski, Š. Višňovský, T. Yamaguchi, J. Eur. Opt. Soc. — Rapid Publ. 1 (2006) 06017-1.
[24] P. Vavassori, Appl. Phys. Lett. 77 (2000) 1605.
[25] H.F. Ding, S. Pütter, H. Oepen, J. Kirschner, J. Magn. Magn. Mater. 212 (2000) 5.
[26] C. Daboo, J.A.C. Bland, R.J. Hicken, A.J.R. Ives, M.J. Baird, M.J. Walker, Phys. Rev. B 47 (1993) 11852.
[27] H.F. Ding, S. Pütter, H.P. Oepen, J. Kirschner, Phys. Rev. B 63 (2001) 134425-1.
[28] T. Mewes, H. Nembach, M. Rickart, B. Hillebrands, J. Appl. Phys. 95 (2004) 5324.
[29] P.B. Johnson, R.W. Christy, Phys. Rev. B 9 (1974) 5056.
[30] Š. Višňovský, M. Nývlt, V. Parízek, P. Kielar, V. Prosser, R. Krishnan, IEEE Trans. Magn. 29 (1993) 3390.
[31] M. Nývlt, M. Przybylski, J. Grabowski, J. Kirschner, J. Appl. Phys. 98 (2005) 033516.
[32] K.-S. Lee, D.-E. Jeong, S.-K. Kim, J.B. Kortright, J. Appl. Phys. 97 (2005) 083519.
[33] S.-K. Kim, K.-S. Lee, J.B. Kortright, S.-C. Shin, Appl. Phys. Lett. 86 (2005) 102502.
[34] F. Stobiecki, M. Urbaniak, B. Szymanski, J. Dubowik, P. Kuswik, M. Schmidt, T. Weis, D. Engel, D. Lengemann, A. Ehresmann, I. Sveklo, A. Maziewski, Appl. Phys. Lett. 92 (2008) 012511.
[35] O. Životský, K. Postava, K. Hrabovská, A. Hendrych, J. Pištora, L. Kraus, Appl. Surf. Sci. 255 (2008) 3322.
[36] J. Hamrlová, K. Postava, O. Životský, D. Hrabovský, J. Pištora, P. Švec, D. Janičkovič, A. Maziewski, *Ellipsometric selective sensitivity to magnetic nanostructures*, Acta Phys. Polonica A 118 (2010) 838.
[37] G. Strang, Introduction to linear algebra, Wellesley Cambridge Press, Wellesley, MA, 2000.
[38] Z. Dostál, Optimal quadratic programming algorithms: with applications to variational inequalities, number 23 in Springer optimization and its applications, Springer, 2009.
[39] A. Stupakiewicz, Z. Kurant, A. Maziewski, L.T. Baczewski, A. Maneikis, A. Wawro, J. Magn. Magn. Mater. 290–291 (2005) 242.